Improved Estimation of Tissue Noise Power Spectra in CT Data

Petr Walek
Dept. of Biomedical Engineering
Brno University of Technology
612 00, Brno, Czech Republic
walek@feec.vutbr.cz

Jiri Jan
Dept. of Biomedical Engineering
Brno University of Technology
612 00, Brno, Czech Republic
jan@feec.vutbr.cz

Petr Ourednicek
Dept. of Imaging Methods
University Hospital St. Anna,
Medical Fac. of Masaryk Uni.
656 91, Brno, Czech Republic
petr.ourednicek@philips.com

Jarmila Skotakova
Children's Hospital - Faculty Hospital
Masaryk University
625 00, Brno, Czech Republic
jskotakova@fnbrno.cz

Igor Jira
Children's Hospital - Faculty Hospital
Masaryk University
625 00, Brno, Czech Republic
igor.jira@fnbrno.cz

ABSTRACT

Evaluation and measuring of image quality in X-ray computed tomographic (CT) data gained importance with recent appearance of modern algorithms for iterative reconstruction of CT data. Thanks to the ability of dramatically reducing applied radiation dose declaratively without loss of image quality, they are expected to replace the conventionally used filtered back projection (FBP) algorithm. Quality of iteratively reconstructed data in terms of image noise is routinely evaluated in images of homogeneous phantoms or in small regions of interest in real patient data. Character of the noise, whose characteristics are dependent on imaged scene, require measuring in the whole volume of real patient data and moreover in diverse tissues separately. This paper presents generalization of one dimensional noise power spectra estimation which enables its calculation from separate tissues. Firstly, basic tissues must be segmented and the resulting segmentation masks are used for the noise power spectra estimation. The estimation carried out with the help of the binary segmentation masks is, due to convolutional property of the Fourier transform, burdened by error due to spectral leakage. A binary segmentation mask may be seen as a two-dimensional windowing function with steep borders. Our method for reduction of the error is based on replacement of binary segmentation masks by designed two-dimensional spatially adaptive windowing functions with better spectral properties. Design of the spatially adaptive windows is based on distance maps and optimized skeletonization calculated using the maximal discs approach. The magnitude of the segmentation introduced error can be experimentally measured using a simulated noise with known power spectrum, which is compared with the noise power spectrum estimated in frame of the segmented tissue (i.e. affected by the spectral leakage). Finally, it is shown that the proposed two-dimensional spatially adaptive windowing functions are able to significantly improve precision of the noise power spectra estimation in diverse tissues.

Keywords

X-ray computed tomography, iterative reconstruction, image quality, noise power spectra, spectral leakage, 2D windowing function.

1 INTRODUCTION

Reduction of radiation dose applied during medical X-Ray computed tomography (CT) imaging is a very topical theme nowadays and many new hardware and software approaches and solutions have been recently introduced in this branch. Significant progress has been made by introduction of modern iterative methods for reconstruction of image data from measured projections which are able to replace conventionally used filtered back projection algorithm (FBP) [BKK12]. Enabling reduction of applied dose up to 70%, declaratively without affecting image quality, makes iteratively reconstructed images very attractive for evaluation of image quality and comparison with quality of images reconstructed by FBP.

Objective quality evaluation of iteratively reconstructed images is, according to recently published studies,

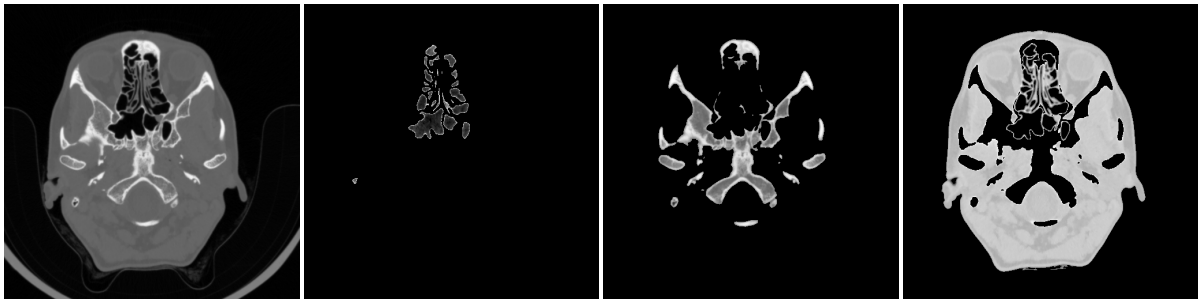

(a) (b) (c) (d)

Figure 1: Exemplary slice from segmentation of head data into three tissues. Binary masks resulting from segmentations are, for illustration, multiplied with original image: (a) original data, (b) segmentation of paranasal sinuses, (c) segmentation of bones, (d) segmentation of soft tissue.

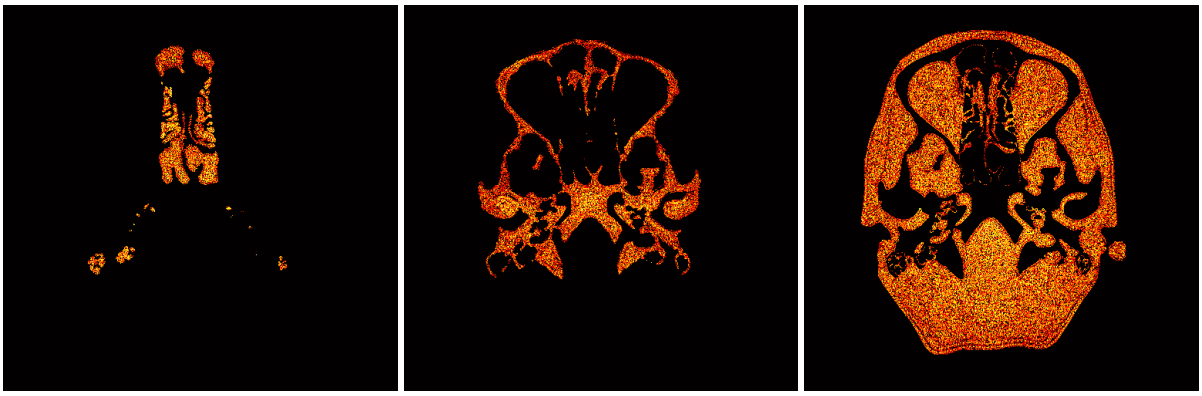

(a) (b) (c)

Figure 2: Examples of residual noise images resulting from subtraction of iteratively and by FBP reconstructed data. The images are for clarity visualized in logarithmic scale and false colors: (a) residual noise in paranasal sinuses, (b) residual noise in bones, (c) residual noise in soft tissue.

based either on evaluation of small homogeneous regions of interest in real patient data [MNS+10], [WTZ+13] or on measuring in imaged artificial phantoms [MGB+13], [GOS12]. Latest studies indicate that noise, a crucial aspect determining image quality, in iteratively reconstructed CT images is object dependent, i.e. noise characteristics are different in diverse tissues, thus mentioned approaches seem to be suboptimal as they are obviously unable to take into account whole complexity of image noise [SS13].

This paper describes a part of a bigger project which aims to extraction and quantitative evaluation of noise parameters from the whole volume of real patient CT data and moreover from diverse tissues. The evaluation of errors in estimation of one-dimensional noise power spectra (a basic characteristic of the CT image noise) in separate tissues, caused by the tissue segmentation, constitutes the core of this work together with a proposal of a method for an error reduction based on two-dimensional spatially adaptive windowing functions. Proposed optimal design of 2D spatially adaptive weighting functions gives possibility to estimate one-dimensional noise power spectra more precisely which will subsequently ease comparison of the noise properties between between separate tissues and also between diverse reconstruction algorithms.

2 PREPROCESSING AND NOISE POWER SPECTRA COMPUTATION

In order to be able to evaluate noise properties in separate tissues, two preprocessing steps must be performed. Anatomical structures must be removed to obtain images of pure noise and basic tissues, whose inherent noise parameters will be further analyzed, must be segmented. As the segmentation algorithm used for distinction between basic tissues do not constitute core of the paper, only the main processing pipeline is stated here; interested reader may find further details in [WJ12]. First step is one-dimensional Top Hats transform based detection of peaks, representing separate tissues, in the gray-scale histogram calculated from whole volume of data. Parameters of detected peaks are further used as initial values for optimal fitting of the histogram by a set of Gaussian curves, which serve for calculation of final thresholds. Simple thresholding

is, due to overlapping of Hounsfield units, unable to distinguish between soft tissues and trabecular bone parts. However, these tissues can be segmented thanks to distinct texture of trabeculae, which significantly changes shape of local histograms in trabecular bone parts. Exemplary segmentation of data from head body part into three main tissues (paranasal sinuses, bones and soft tissue) can be seen in Fig. 1. Providing that anatomical structures are identical in the iteratively and by FBP reconstructed images (both reconstructions must, of course, be calculated from the same raw data), they can be completely removed by subtraction. Images resulting from subtraction of iteratively and by FBP reconstructed images are called residual noise images; after multiplication with binary segmentation masks noise parameters inherent to basic tissues can be extracted from them, see Fig. 2.

Quality of CT images is mostly influenced by radiological noise, composed of quantum and electronic noise, and streaking artifact, a result of passing of X-ray beam via structures with high attenuation (e.g. shoulders of hips) [IIEN10]. The paper is focused only on methodology for estimation of radiological noise parameters, thus only images from head body part are processed as they, according to [BCK$^+$04], do not contain any structures likely to produce streaking artifact.

Basic parameter of radiological noise is its standard deviation which provides an information about typical noise magnitude, but says nothing about noise spectral distribution. Such information is provided by calculation of one-dimensional noise power spectra (1D NPS), the parameter routinely used as an image quality measure in medical CT imaging. Power spectra of residual noise images can be calculated using equation

$$\mathbf{S}(f_x,f_y) = \frac{b_x b_y}{L_B} \cdot \left\langle \left| DFT_{2D}\left\{\mathbf{D}(x,y) - \mathbf{D}_{filt}(x,y)\right\}\right|^2 \right\rangle, \quad (1)$$

$$L_B = \sum_{x=1}^{L_x}\sum_{y=1}^{L_y} \mathbf{B}(x,y)^2, \quad (2)$$

where each slice of three-dimensional noise data $\mathbf{D}(x,y)$ is considered to be a realization of a stochastic field. Data must be zero mean detrended prior to computation of 1D NPS, thus an image filtered by a low pass Gaussian filter $\mathbf{D_{filt}}(x,y)$ is subtracted. Squaring absolute value of two-dimensional Fourier transform, power spectrum of an individual noise realization is obtained. The two-dimensional noise power spectrum of the stochastic field (i.e. a process generating the random noise) is finally calculated as mean value (outlined by $\langle\circ\rangle$ operator) of individual noise power spectra, which is normalized by spatial sampling periods b_x, b_y and by sum of squared values in segmentation mask L_B (segmentation mask need not necessarily be binary and squaring ensures preservation of power in a spectral representation of weighted noise). Power spectra of noise inherent to CT images is rotationally symmetric and its one-dimensional representation (1D NPS) can be, without loss of any information, extracted using radial averaging across a constant absolute spatial frequency.

3 EVALUATION OF SEGMENTATION ERRORS

1D noise power spectra are burdened by error thanks to multiplication of individual noise realizations with segmentation masks which according to convolutional property of the Fourier transform corresponds to convolution of their spectra. Magnitude of this specific kind of error (in frame of this paper called *segmentation introduced error* (SIE)) can be experimentally evaluated using the following procedure. A three-dimensional matrix completely filled by white noise is generated and subsequently colored (its noise spectrum weighted) by an artificially generated function. 1D NPS calculated

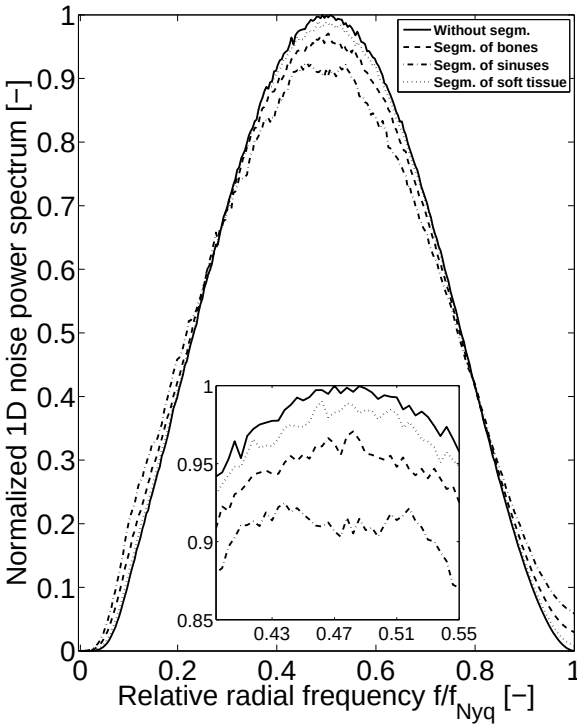

Figure 3: Example of 1D NPS estimation errors introduced by segmentation of basic tissues: solid line (——) 1D NPS unaffected by segmentation (gold standard), dotted line ($\cdots$) 1D NPS affected by segmentation of soft tissue, dash-dotted line ($-\cdot-$) 1D NPS affected by segmentation of paranasal sinuses, dashed line ($-\,-\,-$) 1D NPS affected by segmentation of bones.

from this matrix is unaffected by a segmentation mask and will thus serve as a gold standard for evaluation of SIE (see solid line in Fig. 3). The noise matrix is multiplied with a segmentation mask and the 1D NPS calculated from the result is therefore affected by segmentation (see dotted, dashed and dash-dotted lines in Fig. 3). Final vector of SIE (each vector sample represents a discrete absolute spatial frequency) is calculated as absolute value of difference between the gold standard and 1D NPS affected by segmentation.

Errors in estimation of 1D NPS introduced by segmentation of basic tissues (using binary segmentation masks) were quantitatively assessed in [WJO+13]. Findings resulting from the analysis of a group of 40 brain images are following: mean SIE is under 1% for soft tisssue, under 4% for bones and under 7% for paranasal sinuses, but in idividual cases (for a specific patient at a concrete frequency) SIE can be even higher than 25%. Reduction of segmentation introduced error during estimation of 1D NPS (i.e. estimation precision improvement) is therefore an actual and challenging problem.

4 METHOD FOR REDUCTION OF SEGMENTATION ERRORS

Errors introduced by segmentation are caused by so-called spectral leakage, the effect well known from one dimensional signal processing where shortening of theoretically infinite signal by a rectangular window causes decrease of frequency resolution and leakage as signal spectrum is convolved with spectrum of weighting window (i.e. sinc function). Undesirable effect of leakage in spectral domain is usually reduced either by prolonging the window length or using a window with better spectral properties. Analogically, binary segmentation mask can be viewed as a two-dimensional rectangular weighting window with spatially adaptive shape. Shape of binary segmentation mask is fixed by delineation of tissue. Prolonging of window length therefore can not be used and the only chance for reducing spectral leakage is in designing of two-dimensional windowing functions in analogy to those commonly used in signal processing (e.g. Hann or Hamming) but with ability to adapt its shape to a shape of segmented binary object.

4.1 Design of two-dimensional spatially adaptive windowing functions

Common one-dimensional weighting windows are real, even, nonnegative and time limited functions of one variable n (index of sample in the window) and one parameter N (width of windowing function); see equation 3 for computation of the Hann window [Har78].

$$w(n) = 0.5 \left[1 - \cos\left(\frac{2\pi n}{N} \right) \right]. \qquad (3)$$

Situation is rather complicated in two dimensions especially due to locally varying width of binary objects; N is thus no longer a parameter and becomes a variable reflecting unequal shape of binary objects. Variable n can be in two-dimensional case represented by values of Euclidean distance map [Soi03]

$$D(f)\Big|_{i,k} = \min \left\{ d_e\left((i,k),(m,n)\right) \Big| f_{m,n} = 0 \right\}, \qquad (4)$$

which for each active (nonzero) image pixel $f_{i,k}$ calculates Euclidean distance d_e to the nearest zero-valued pixel $f_{m,n}$, see e.g. the distance map (Fig. 4b) of an elliptically-shaped binary object (Fig. 4a). Concept of distance maps can be also used to calculate local width of binary objects, and thus a variable N. Having defined a medial axis g of a binary object as a set of points with more than one closest points to the object's boundary (see Fig. 4a where medial axis, a line of active pixels, is subtracted from binary object), parametric map of distances to closest points of medial axis can be calculated (Fig. 4c). Sum of two linear functions with mutually opposite slopes gives a constant function with height equal to sum of their y-intercepts. As distance map is a linear function and maps of distances to object's border and medial axis have opposite slopes (see dashed and doted lines in Fig. 5a), identical property is used and the resulting constant function corresponds to the local width (see dash-dotted line in Fig. 5a). In other words; for each pixel, sum of its distance to an object's border and distance to a closest point of medial axis gives a local width.

Map of distances to closest points of medial axis can be effectively obtained by placing set of ones representing medial axis onto zero background, calculating inverse distance map (for each zero pixel calculate distance to closest active pixel) according to equation 5, and multiplying with original binary object.

$$\tilde{D}(g)\Big|_{i,k} = \min \left\{ d_e\left((i,k),(m,n)\right) \Big| g_{m,n} = 1 \right\}. \qquad (5)$$

Map of distances to closest points of medial axis can be seen in Fig. 4c and map of local widths (sum of $D(f)$ and $\tilde{D}(g)$) in Fig. 4d. Final 2D *spatially adaptive window* (SAW) is calculated substituting variables n and N onto one-dimensional formula calculating half (from ridge to border) of windowing function, see Fig. 4e.

Using fast algorithms for distance transforms [MR03] and having possibility to calculate 2D windowing functions effectively in matrix notation, creation of spatially adaptive windowing functions do not constitute significant computational burden. Position of object's medial axis needs to be known for proper calculation of local widths map. This can be approximated by binary skeleton, the result of a skeletonization algorithm.

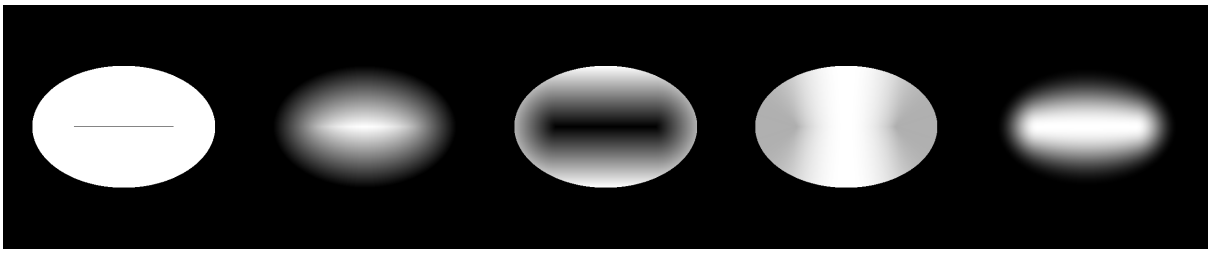

(a) (b) (c) (d) (e)

Figure 4: Design of a two-dimensional spatially adaptive weighting function: (a) original binary object with elliptic shape (length of major and minor axis are 384 px and 256 px, respectively, in 512×512 px sized image), medial axis of the object is delineated by a black line (180 px long; centered on major axis) inside the object, (b) distance map of the binary object; variable n in Eq. 3, (c) map of distances to closest points of medial axis, (d) map of local widths; variable N in Eq. 3, (e) final two-dimensional spatially adaptive Hann windowing function.

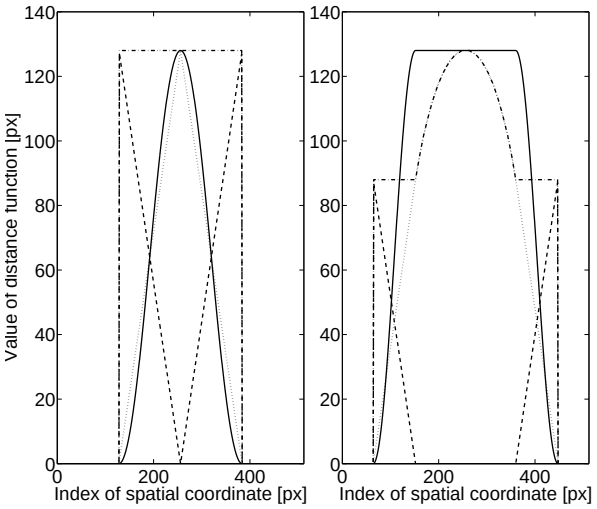

(a) (b)

Figure 5: Cross-sections of figures from Fig. 4b to Fig. 4e taken along minor (a) and major (b) axis, plotted as one-dimensional signal: dotted line ($\cdots$) cross-section of distance map; dashed line ($- - -$) cross-section of map of distances to closest points of medial axis; dash-dotted line ($- \cdot -$) cross-section of local widths map; solid line (——) cross-section of two-dimensional spatially adaptive Hann window (in order to fit on axis of the plot multiplied with maximum of local widths).

4.2 Suppression of segmentation introduced error using 2D SAW

Many approaches and algorithms for extraction of skeleton (grass-fire propagation, thinning algorithms, distance transform or maximal disk based approaches etc.) are routinely used in image processing, especially in character recognition and shape analysis [Soi03]. Diverse skeletonization algorithms give, in general, different skeletons; skeletonization can moreover be sensitive to gentle variations in object's shape and skeleton thus can contain many redundant (in a sense of local widths map calculation) branches. The question now posed is how to perform skeletonization to be as suitable as possible for calculation of a local widths map. Initially, a homotopic skeleton generated by sequential thinning using structure elements from the Golay alphabet (implemented in MATLAB® software package) is applied.

Having defined a skeleton of binary object and using methodology described in section 3, a quality of the 1D NPS estimation (i.e. the magnitude of segmentation introduced error) using spatially adaptive weighting functions can be evaluated, and directly compared with the quality when using the respective binary masks. Thirteen types of windowing functions (Bartlett, Welch, Hann, Hamming, Blackman, Nuttall, Blackman-Nuttall, Blackman-Harris, flat top, Gaussian, exponential, Bartlett-Hann, Hann-Poisson and Lanczos) have been tested, but results are presented only on five functions which seem to be the most suitable for this application. Overall SIE (i.e. one vector of errors 256×40 samples long; 256 errors on axis of absolute spatial frequencies for 40 brain images) for the three basic tissues are visualized in Fig. 7 in form of box plots.

According to Fig. 7b and Fig. 7c, reduction of segmentation introduced error can be achieved by substituting binary masks with 2D SAW in cases where 1D NPS of bones and soft tissue are estimated. Using 2D SAW seems not to have substantial positive effect on 1D NPS estimation of paranasal sinuses, see Fig. 7a, moreover usage of some windowing functions (e.g. Bartlett) exhibit even greater SIE than usage of rectangular windows. Pure Euclidean distance maps calculated directly from binary segmentation masks can be also used as a kind of 2D windows and they exhibit favorable properties, see box plots marked as "Distance" in Fig.7.

The possible explanation why Euclidean distance functions exhibit better properties than 2D SAW lies in

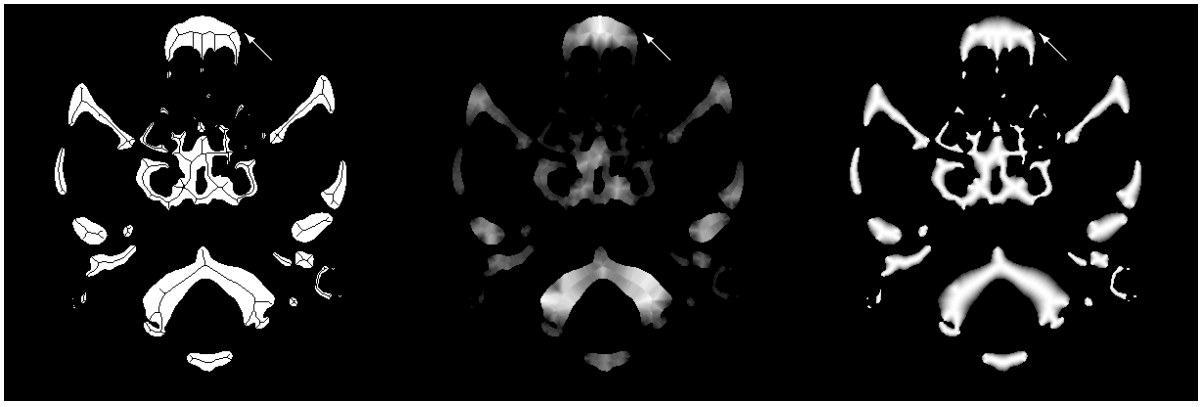

(a) (b) (c)

Figure 6: A two-dimensional spatially adaptive weighting function of a real skeletal structure calculated using skeletonization based on sequential thinning with structure elements from the Golay alphabet: (a) skeleton subtracted from binary segmentation mask of bones, (b) map of local widths, (c) spatially adaptive Welch window.

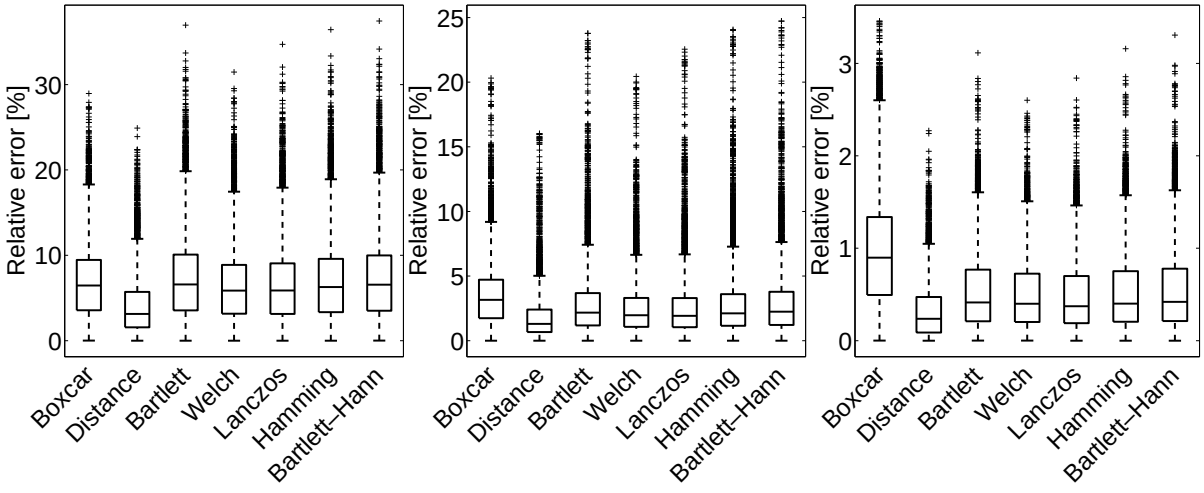

(a) (b) (c)

Figure 7: Overall 1D NPS estimation error introduced by segmentation of basic tissues visualized in form of box plots (lower adjacent value - 25th percentile - median - 75th percentile - upper adjacent value - outliers); two-dimensional spatially adaptive weighting functions of different types, designed using homotopic skeleton based on sequential thinning, are used: (a) paranasal sinuses, (b) bones, (c) soft tissue.

used type of skeletonization algorithm. Skeleton generated by sequential thinning is not suitable for calculation of local widths map as it contains many redundant branches which moreover have endpoints very close to object's border. Branches of skeleton near to an object's border cause decrease of local width and false ridges of 2D SAW are subsequently generated (see arrows in Fig 6).

Bartlett 2D SAW have, using identical skeletonization, worse properties than other windowing functions (e.g. Welch or Lanczos), see Fig. 7. Regardless that Euclidean distance and Bartlett function have an identical character (i.e. linear function), Bartlett 2D SAW have worse properties. A skeleton which meets the condition that resulting Bartlett 2D SAW is maximally similar to distance map can be designed and Welch or Lanczos 2D SAW calculated using such skeleton may have better properties, and thus lower SIE, than distance function.

4.3 Optimized skeletonization

To be able to design skeleton optimally, in a sense that created Bartlett SAW is maximally similar to distance map, skeletonization algorithm must allow to control shape and properties of skeleton by some parameter. Skeletonization method which satisfies this condition is based on maximal disks [CLS03], where skeleton is represented by a set of centers of maximal disks inscribed into binary object.

Disk B inscribed into object is maximal if there is no other inscribed disk which contains disk B. In other

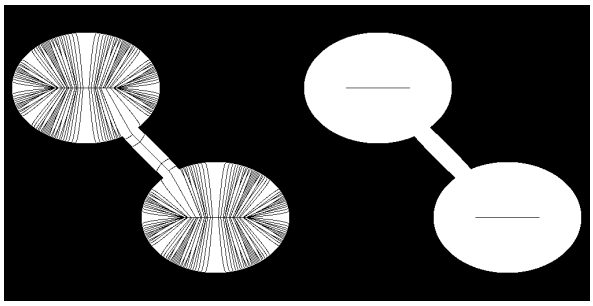

(a) (b)

Figure 8: Effect of parameter ρ setting to a maximal discs based skeletonization demonstrated on synthetic binary image: (a) skeleton with low ρ parameter ($\rho = 3$), (b) skeleton with high ρ parameter ($\rho = 50$).

words, maximal disk of object X, with center in position $\mathbf{x}$, must touch object's border in two sufficiently distinct points $\mathbf{y_1}$ and $\mathbf{y_2}$. Minimum distance between the two contour points for considering a disk to be maximal is determined by a parameter ρ. Formally, a maximal disk of an object X with center in a point $\mathbf{x}$ (the part of skeleton $SK(X)$) can be expressed by formula

$$\mathbf{x} \in SK(X) \Leftrightarrow \exists\, \mathbf{y_1}, \mathbf{y_2} \in \delta X \mid d_e(\mathbf{y_1}, \mathbf{y_2}) \geqslant \rho \text{ and } d_e(\mathbf{x}, \delta X) = d_e(\mathbf{x}, \mathbf{y_1}) = d_e(\mathbf{x}, \mathbf{y_2}), \quad (6)$$

where δX denotes the boundary of X and d_e expresses Euclidean distance.

The choice of parameter ρ can significantly influence properties of a skeleton, see two skeletons of identical binary object with differently adjusted ρ in Fig. 8. The choice must follow compromise between creation of many redundant branches if low ρ is used, see Fig. 8a, and between intrusion of a skeleton into thin sections of a binary object, see Fig. 8b.

Due to complex shape of objects representing segmented tissue, it is impossible to identify one optimal value of ρ to generate the skeleton which meets the condition that created Bartlett 2D SAW is maximally similar to object's distance map. Optimal skeleton must therefore be calculated in iterative manner. Initially, the skeleton is calculated with relatively high ρ, set to maximum of object's distance map, which provides its fundamental part in thick parts of the object without any redundant branches. A 2D Bartlett SAW is calculated from the basic skeleton and its similarity, in terms of normalized cosine criterion calculated between two matrices reformatted to vectors, to object's distance map is calculated. In each other iteration, skeletonization with lower parameter ρ (geometrically decaying with 0,9 exponent) is calculated and new branches of the skeleton arises. The new branches are extracted, each branch is individually connected with actual skeleton, and new similarity criterion with distance map is calculated. If criterion rises, the branch contributes to better similarity with distance map and is permanently connected to the skeleton. Otherwise the branch is discarded and can not be used in further iterations.

Skeleton created using described iterative scheme do not include any redundant branches and may not necessarily be connected, see Fig.11a. Corresponding map of local widths is much smoother than one derived from skeleton based on iterative thinning, compare Fig. 11b and Fig. 6b, and also final Welch 2D SAW contains, in contrast to previously used skeletonization, fewer false ridges, see Fig. 11c.

4.4 Comparison of Computation Times

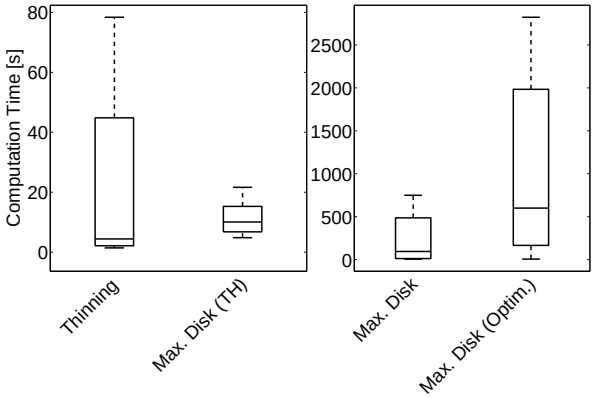

(a) (b)

Figure 9: Computation times of used skeletonization algorithms visualized in form of box plots (lower adjacent value - 25$^{\text{th}}$ percentile - median - 75$^{\text{th}}$ percentile - upper adjacent value): "Thinning" - sequential thinning; "Max. Disk" - original maximal disk based skeletonization; "Max. Disk (TH)" - speed-up by Top Hats transform; "Max. Disk (Optim.)" - proposed optimized skeletonization.

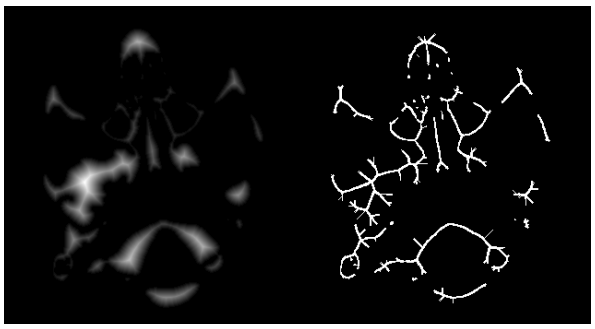

(a) (b)

Figure 10: Extraction of distance map ridges based on 2D Top Hats transform: (a) distance map, (b) binary labeling of detected distance map ridges.

(a) (b) (c)

Figure 11: A two-dimensional spatially adaptive weighting function of a real skeletal structure calculated using optimized skeletonization based on maximal discs: (a) skeleton subtracted from binary segmentation mask of bones, (b) map of local widths, (c) spatially adaptive Welch window.

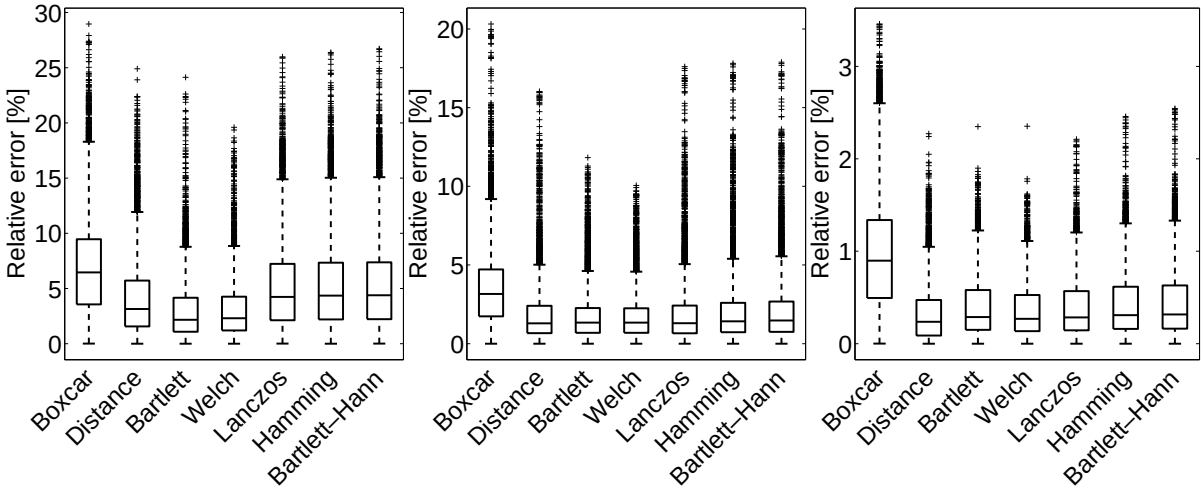

(a) (b) (c)

Figure 12: Overall 1D NPS estimation error introduced by segmentation of basic tissues visualized in form of box plots (lower adjacent value - 25$^{\text{th}}$ percentile - median - 75$^{\text{th}}$ percentile - upper adjacent value - outliers); two-dimensional spatially adaptive weighting functions of different types, designed using optimized skeleton based on maximal discs, are used: (a) paranasal sinuses, (b) bones, (c) soft tissue.

Having a skeleton of a binary object defined creation of 2D SAW do not constitute, as stated in section 4.1, significant computational burden. Overall computation time of 2D SAW is thus mostly dependent on computation time of used skeletonization algorithm. Computation times of the skeletonization algorithms (thinning and maximal discs based) are compared in this section and adjustment for speed-up of finally proposed optimized skeletonization is proposed. Fig. 9 shows computation times of used skeletonization algorithms measured during skeletonization of the segmented tissues on whole set of the available data. The measurements have been conducted on workstation with 2×Intel Xeon CPU @ 2,53 GHz with 48 GB RAM.

According to the resulting computation times, skeletonization based on maximal disks is approximately 10 times more time consuming than thinning algorithm. Maximal disk skeletonization is based on testing of individual active pixels in binary image and decision whether they are centers of maximal discs or not. As the optimal medial axis likely lies near to ridges of the object's distance maps, the proposed methodology do not require testing of each binary object's active pixel. Testing of active pixels situated only near to distance map ridges can thus speed-up the skeletonization. Distance map ridges are extracted by means of two-dimensional Top Hats transform [Soi03] performed using four (three pixels long and line shaped) structure elements (each of them inclined by 0 °, 45 °, 90 ° and 135 °). The four resulting parametric images are summed and pix-

els with nonzero value are considered as candidates for skeletonization, see Fig. 10b. Maximal disk based skeletonization with initialization by Top Hats transform is, according to Fig. 9, very fast and even faster than method based on thinning.

Proposed optimized skeletonization is, despite its speed-up by Top Hats transform, very time consuming compared to use of thinning based skeletonization, see Fig. 9. Increased computation time is a logical result of iterative manner of optimized skeletonization where several operations (skeletonization with different ρ parameter, identification of new skeleton branches, calculation of the similarity criterion etc.) are repeated.

5 RESULTS

Comparison of overall segmentation introduced errors using spatially adaptive windowing functions derived from thinning based skeletonization and optimized skeletonization based on maximal disks can be made on box plots in Fig. 7 and Fig. 12. The box plots are computed from statistically respectable set of 40 patients and the improvement is clear in each tissue of interest. It can be concluded that use of proposed optimized skeletonization leads to significantly smaller SIE compared to use of binary segmentation masks and also to use of 2D SAW designed from thinning based skeleton. Improvement of SIE is evident for each tissue of interest, but the most apparent is in case of paranasal sinuses. Comparing the results for the tested windowing functions it can be observed that differences in quality of 1D NPS estimation between them are similar regardless of tissue of interest or used skeletonization (e.g. Hamming and Bartlett - Hann window have always similar results and Welch window is always the best). Properties (most probably frequency properties) of individual windowing function thus plays significant role in this application which can be further utilized.

Improvement of segmentation introduced errors using proposed 2D SAW with optimized maximal disk based skeletonization is evident but for the price of significantly higher computation time, see box plots in Fig. 9.

6 CONCLUSIONS AND FUTURE WORK

The novel method for improved estimation of tissue one-dimensional noise power spectra is presented in this paper. The improvement lies in reduction of errors introduced by segmentation of basic tissues and is based on design of two-dimensional spatially adaptive windowing functions which replace binary segmentation masks. Resulting segmentation introduced errors, presented by box plots in Fig. 12, demonstrate substantial decrease of the errors while using 2D SAW compared to errors caused by binary segmentation masks.

Despite the evident decrease of tissue 1D NPS estimation errors, perspectives for further improvement, and even more precise estimation of 1D NPS, can be seen. Skeleton, which is crucial for design of 2D SAW and also for final magnitude of SIE (compare box plots in Fig.7 and Fig.12), is in this paper calculated optimally such that the resulting Bartlett (triangular) SAW is maximally similar to the distance map of the original object. The original idea assumes that such optimal skeleton design will exhibit equal SIE for Bartlett SAW and distance maps. Use of better windowing functions (windows which exhibit less error than Bartlett while non-optimized skeletonization is used) on those skeletons will thereafter decrease SIE below the level of error when distance maps are used. The idea is not fully confirmed as errors produced by Bartlett windows while estimating 1D NPS of paranasal sinuses are substantially lower than SIE while using distance maps, see Fig.12a, and higher in case of soft tissue, see Fig.12c. Those discrepancies suggest that skeletonization can be performed in such way that segmentation introduced error of Bartlett 2D SAW is lower than error produced by distance maps, which gives a good perspective for future work.

In order to achieve even more precise estimation of tissue 1D NPS, skeletonization will not be further optimized on the basis of similarity with a distance map. One possible alternative way is to optimize theoretical frequency properties of windowing functions. Measuring frequency properties of one-dimensional windowing functions is well known problem, see [Har78], and many parameters such as peak ripple value of sidelobes, the frequency at which main lobe drops to the peak ripple value of sidelobes, bandwidth of main lobe at attenuation -3 dB and -6 dB, sidelobes fall off rate or equivalent noise bandwidth are routinely used. It is possible to generalize those parameters and use them in two-dimensional case. Which frequency parameters are appropriate for tissue 1D NPS estimation remains to be found, theoretical assessment of windows quality must therefore be coupled with practical measures based on simulated noise as described in section 3. Determination of crucial frequency parameters will be performed on a set of testing binary images, similar to the binary object in Fig. 8, specially designed to find out whether intrusion of skeleton into thin parts of binary objects is advantageous.

An alternative to the proposed two-dimensional spatially adaptive weighting functions can be represented by 2D tapered windows (inspired by Tukey function [Har78]), which modulate the function smoothly to zero only at the boundaries of an object. Such a 2D window can be created using certain number of morphological thinning iterations applied to a binary object and subsequent 2D convolution with properly scaled 2D kernel (e.g. Hann window as function of two spatial variables).

This approach will also require optimization; i.e. optimization of the number of thinning iterations which influence depth of binary object's border modulation.

The proposed methodology of designing 2D spatially adaptive windowing functions may possibly have further applications, e.g. in texture analysis based on locally calculated Fourier transforms. Use of the proposed windowing functions may then enable more precise calculation of texture features in locations where Fourier transform can not be calculated from square neighborhood (for example in detection of retinal nerve fibre layer near to vessels in fundus camera images).

7 ACKNOWLEDGMENTS

Lending of the iDose and IMR reconstructor prototype programme packages from Philips Healthcare is highly acknowledged as well as the long term data acquisition enabled by the Brno Faculty Hospital, Children's Radiology Department.

8 REFERENCES

[BCK+04] A. J. Britten, M. Crotty, H. Kiremidjian, A. Grundy, and E. J. Adam. The addition of computer simulated noise to investigate radiation dose and image quality in images with spatial correlation of statistical noise: an example application to X-ray CT of the brain. *British Journal of Radiology*, 77(916):323–328, April 2004.

[BKK12] Marcel Beister, Daniel Kolditz, and Willi A. Kalender. Iterative reconstruction methods in X-ray CT. *Physica medica : PM : an international journal devoted to the applications of physics to medicine and biology : official journal of the Italian Association of Biomedical Physics (AIFB)*, 28(2):94–108, April 2012.

[CLS03] Wai-Pak Choi, Kin-Man Lam, and Wan-Chi Siu. Extraction of the Euclidean skeleton based on a connectivity criterion. *Pattern Recognition*, 36(3):721–729, March 2003.

[GOS12] C. Ghetti, O. Ortenzia, and G. Serreli. CT iterative reconstruction in image space: A phantom study. *Physica medica : PM : an international journal devoted to the applications of physics to medicine and biology : official journal of the Italian Association of Biomedical Physics (AIFB)*, 28(2):161–5, April 2012.

[Har78] F.J. Harris. On the use of windows for harmonic analysis with the discrete Fourier transform. *Proceedings of the IEEE*, 66(1):51–83, 1978.

[IIEN10] Kuniharu Imai, Mitsuru Ikeda, Yukihiro Enchi, and Takanaga Niimi. A detection method for streak artifacts and radiological noise in a non-uniform region in a CT image. *Physica medica : PM : an international journal devoted to the applications of physics to medicine and biology : official journal of the Italian Association of Biomedical Physics (AIFB)*, 26(3):157–65, January 2010.

[MGB+13] Frédéric A. Miéville, François Gudinchet, Francis Brunelle, François O. Bochud, and Francis R. Verdun. Iterative reconstruction methods in two different MDCT scanners: physical metrics and 4-alternative forced-choice detectability experiments–a phantom approach. *Physica medica : PM : an international journal devoted to the applications of physics to medicine and biology : official journal of the Italian Association of Biomedical Physics (AIFB)*, 29(1):99–110, January 2013.

[MNS+10] Daniele Marin, Rendon C. Nelson, Sebastian T. Schindera, Samuel Richard, Richard S. Youngblood, Terry T. Yoshizumi, and Ehsan Samei. Low-tube-voltage, high-tube-current multidetector abdominal CT: improved image quality and decreased radiation dose with adaptive statistical iterative reconstruction algorithm–initial clinical experience. *Radiology*, 254(1):145–53, January 2010.

[MR03] C.R. Maurer and Vijay Raghavan. A linear time algorithm for computing exact Euclidean distance transforms of binary images in arbitrary dimensions. *IEEE Transactions on Pattern Analysis and Machine Intelligence*, 25(2):265–270, February 2003.

[Soi03] Pierre Soille. *Morphological image analysis*. Springer Verlag, Berlin, 2003.

[SS13] Justin Solomon and Ehsan Samei. Are uniform phantoms sufficient to characterize the performance of iterative reconstruction in CT? In *Proc. SPIE 8668, Medical Imaging 2013: Physics of Medical Imaging*, March 2013.

[WJ12] Petr Walek and Jiri Jan. Segmentation of basic tissues for assessing noise in iteratively reconstructed MDCT data. In *Advances in Sensors, Signals, Visualization, Imaging and Simulation*, pages 211–216. WSEAS Press, 2012.

[WJO+13] Petr Walek, Jiri Jan, Petr Ourednicek, Jarmila Skotakova, and Igor Jira. Methodology for Estimation of Tissue Noise Power Spectra in Iteratively Reconstructed MDCT Data. In *21st International Conference in Central Europe on Computer Graphics, Visualization and Computer Vision, WSCG 2013 - Full Papers Proceedings*, pages 243–252, Pilsen, 2013.

[WTZ+13] Haiyan Wang, Bingyi Tan, Bin Zhao, Changhu Liang, and Zhuodong Xu. Raw-data-based iterative reconstruction versus filtered back projection: image quality of low-dose chest computed tomography examinations in 87 patients. *Clinical imaging*, 37(6):1024–32, 2013.